Springer

KSME

Journal of Mechanical Science and Technology 24 (12) (2010) 2467~2477
www.springerlink.com/content/1738-494x
DOI 10.1007/s12206-010-0928-9

Numerical estimation of ion transport and electroosmotic flow around a pair of cylindrical electrodes in a microchannel using immersed boundary method †

Dolfred Vijay Fernandes, Sangmo Kang and Yong Kweon Suh*

Department of Mechanical Engineering, Dong-A University, Busan, 604-714, Korea

(Manuscript Received March 24, 2010; Revised July 2, 2010; Accepted August 31, 2010)

Abstract

This paper investigates the ion transport and electroosmotically induced flow around the cylindrical electrodes under both direct current (DC) and alternating current (AC) fields. The Poisson-Nernst-Plank (PNP) equations governing the ion transport around the ideally polarizable electrodes are solved numerically by neglecting the Stern layer effect. The fractional-step (FS) based decoupled solver is used in time integration of the ion-transport equations. A new immersed boundary (IB) methodology is described for imposing no-flux boundary conditions of ion concentration on the electrodes. A fully implicit coupled solver is also developed for calculating the ion transport around a pair of rectangular electrodes. The validity of the decoupled solver is verified by comparing its results with those obtained from the coupled solver. For further confirmation of the validity, the results are also compared with those obtained from the Poisson-Boltzmann model and both results are found to be in excellent agreement. The electroosmotically induced flow field is studied by numerically solving the Stokes equations. The system attains a steady state under DC, where the conduction term of ion transport is balanced by the diffusion term. Until the system attains a steady state for a few ms for the case of DC, fluid flow is induced. The electroosmotic flow under AC is more interesting, in that instantaneous flow oscillates with the frequency double of the applied field and a non-zero steady velocity field persists.

Keywords: Ion transport; Electroosmotic flow; Electric double layer; Immersed boundary method; Poisson-Nernst-Planck equations

1. Introduction

Electroosmotic flow refers to the bulk motion of an aqueous solution induced by the application of an electric field to the surplus charge in the electric double layer (EDL) near a surface. It is a well known fact that when a charged surface is brought in contact with an aqueous solution with free ions, the electrical charges at the surface attract the ions in the fluid that have opposite sign, and a highly concentrated counter-ion layer is formed near the electrode surface. This thin layer with net charge can be dragged by the application of a tangential electric field. In case of microchannels this gives a plug-like flow profile. Many researchers have studied this kind of flow, either making use of the Poisson-Boltzmann assumption or by just considering slip boundary conditions for the velocity [1-5].

For an infinite plain surface in contact with an electrolyte, one can easily study the ion transport and the structure of EDL by making a one-dimensional assumption. There are well known classical theories (such as Gouy-Chapman, Poisson-Boltzmann) depicting the structure of EDL clearly for the one-dimensional case [5-6]. But practically the surfaces coming in contact with an electrolyte may not be infinite or of regular shape. Also, in many engineering applications one comes across the situations where the electrode surface is completely immersed in the electrolyte [7-8]. These cases require multi-dimensional analysis of the ion transport. Obtaining analytical solution in two or three dimensions is not viable due to the non-linearity of ion transport equations and as well as due to their strong coupling with the Poisson equation for the induced potential. Thus, opting for a numerical solution is more economical.

Most of the studies on ion transport are based on thin double layer and Poisson-Boltzmann distribution assumptions. Few researchers have paid attention to the ion transport around the charged surfaces by solving Poisson-Nernst-Planck equations. Yu and Admassu [9] investigated removal of the metal ions in a process stream of the pulp and paper industry by electrodialysis. They obtained an analytical solution of 1D transport of cations and discussed the relationships among metal ion concentration, electrical current density and removal efficiency. The modeling of unidimensional non-steady ion transport in electrochemical systems is proposed by Volgin and Davydov

† This paper was recommended for publication in revised form by Associate Editor Dohyung Lee

* Corresponding author. Tel.: +82 51 200 7648, Fax.: +82 51 200 7656
E-mail address: yksuh@dau.ac.kr

[10], considering the diffusion, migration, convection and homogeneous reaction. In their numerical calculations they had to use very small time steps of the order of 10^{-14} to 10^{-12} seconds. Bazant et al. [11] surveyed the theoretical treatment of ion transport equations in the past and obtained numerical solution of the ion transport for the facing electrodes. Kang and Suh [12] investigated electroosmotic flows in a microchannel with rectangle-waved surface roughness using the PNP model. Recently, Suh and Kang [13] proposed a triple-layer structure for the ion transport near the polarized electrodes under AC.

On the other hand, the cylindrical electrodes used in the present study have complex geometries. So the immersed boundary (IB) method is best suited for this problem, as it has many advantages over conventional adapted grids; e.g., the task of grid generation is the most simplified. At present we can see numerous works done in the field of IB method for fluid flow. The surfaces immersed in the fluid domain are modeled by introducing a virtual body force, generally known as momentum force, into the momentum equations [14-17]. There are many different methodologies for determining and applying the virtual body force. Mittal and Iaccarino [18] classified these momentum forcing techniques into two broad categories. One is the continuous forcing approach where forcing is applied throughout the domain. The other is the discrete forcing approach where forcing is applied to the virtual cells cut by an immersed boundary.

In this paper we describe the ion transport and electroosmotic flow around a pair of cylindrical electrodes. We assume that the electrodes are completely polarizable and the walls of the domain are insulated. Section 2 describes the physical and mathematical model. The PNP equations governing ion transport are solved in a decoupled way. The discrete forcing approach is used to impose the boundary conditions. The momentum forcing values are obtained using the procedure given in Kim et al. [19]. On the other hand, to impose concentration boundary-conditions we have developed a new IB technique which is described in Section 3. The results and discussions are given in Section 4 and the summary of the work is presented in Section 5.

2. Physical and mathematical model

The physical model consists of a long rectangular microchannel with axial electrodes with infinite extent as shown in Fig. 1(a). The purpose of the model selected here is to depict the applicability and correctness of the method presented in the paper and also to investigate the physical phenomenon of electroosmosis. The electrodes are characterized by the ideally polarizable surfaces. The application of the potential difference between the electrodes introduces the lateral electroosmotic flow, which does not produce or perturb the axial flow. Thus, the analysis of ion transport and electroosmotic flow can be done in the section of the channel and the problem reduces to two-dimensional (2D). The computational domain considered in the analysis is shown in Fig. 1(b). The surrounding boundaries are of dimension $10d \times 5d$, where d is the electrode size (Fig. 1). The size of the electrodes d is fixed as 1μm, which is restricted to such a low value because otherwise it may give rise to a relatively very thin double layer around electrodes that would require a large number of grids there.

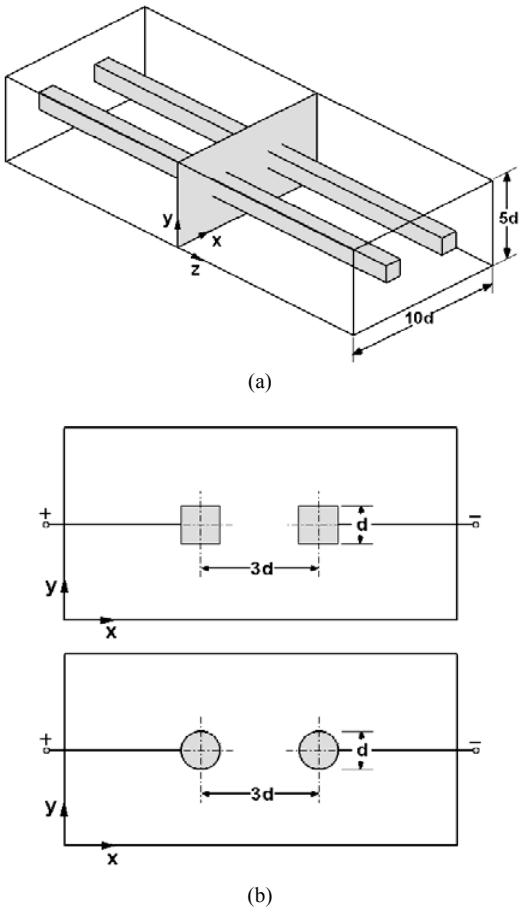

Fig. 1. Schematic diagram of Physical and computational domain (a) microchannel with axial electrodes and (b) x-y section (not to scale).

The mathematical model governing the electric field distribution, ion transport and fluid flow is to be presented. According to the theory of electrostatics, for any general electrolyte consisting of N different ionic species, the relationship between the electrical potential, ψ^*, and the net charge density per unit volume, ρ_e^*, is given by the Poisson equation as follows:

$$\varepsilon\varepsilon_0 \nabla^2 \psi^* = -\rho_e^*, \tag{1a}$$

$$\rho_e^* = \sum_{k=1}^{N} z_k e C_k^*, \tag{1b}$$

where ε is the relative permittivity of the electrolyte, ε_0 permittivity of the vacuum, e the electron charge (1.6×10^{-19} C), and z_k and C_k^* are, respectively, the valence and the ion number

concentration (no. of ions / m^3) of the k^{th} ionic species.

The material balance of ionic species is governed by Nernst-Plank (NP) equations as follows:

$$\frac{\partial C_k^*}{\partial t^*} = -\nabla \cdot \mathbf{J}_k^*, \quad (k = 1,...., N), \tag{2a}$$

$$\mathbf{J}_k^* = -D_k \nabla C_k^* - \frac{z_k F}{RT} D_k C_k^* \nabla \psi^* + \mathbf{V}^* C_k^*, \tag{2b}$$

where $\mathbf{J}_k^*$ and D_k are, respectively, the ionic flux and the diffusion coefficient of k^{th} ionic species and $\mathbf{V}^*$ is the velocity vector of the surrounding fluid.

For the simplification of the problem we make several assumptions. First, the electrolyte is dilute, symmetric and binary and contains only monovalent species ($z_1 = -z_2 = 1$). The diffusion coefficients D_k are constant and independent of the ionic species. The process is non-Faradaic and isothermal, and the properties of the electrolyte remain invariant. The potential drop across the Stern layer is neglected; hence the potential at the shear plane is equal to the applied potential.

Generally, the induced electroosmotic velocities are of the order of 10 to 100 $\mu m/s$. For the selected parameters the Péclet number associated with the advection term comes out to be in the range 10^{-1} to 10^{-2} . From the order of magnitude analysis it is found that the contribution of advection term is 10 to 100 times less compared with the other terms. Hence we have neglected the advection terms in the NP equations (i.e., the last term in Eq. (2b)) during the numerical analysis.

The fluid flow induced in the domain due to the Coulomb force acting on the charge in the EDL is characterized by very low Reynolds number and thus governed by the Stokes equation as follows:

$$\nabla \cdot \mathbf{V}^* = 0, \tag{3}$$

$$\rho \frac{\partial \mathbf{V}^*}{\partial t^*} = -\nabla^* P^* + \mu \nabla^{*2} \mathbf{V}^* - \rho_e^* \nabla^* \psi^*, \tag{4}$$

where P^* , ρ and μ are, respectively, the pressure, density and dynamic viscosity of the electrolyte.

The superscript * in the above equations indicates that the corresponding quantity is in dimensional form. Prior to solving the equations numerically, they are nondimensionalized by scaling the variables as follows: $\mathbf{x}^* = d\mathbf{x}$, $\mathbf{V}^* = U_s \mathbf{V}$, $P^* = P_{ref}^* P$, $t^* = d^2 t / D$, $C_k^* = C_0^* C_k$, $\psi^* = \psi_{ref}^* \psi$, $\rho_e^* = \left(C_0^* z e\right) \rho_e$, where $U_s = \varepsilon \varepsilon_0 \varsigma V_{apo} / \mu d$ is the Helmholtz-Smoluchowski velocity. The reference pressure is defined as $P_{ref}^* = \rho U_s D / d$ and the reference potential as $\psi_{ref}^* = \left(d / \lambda_d\right)^2 \varsigma / 2$. Further, λ_d is Debye screening length defined as $\sqrt{\varepsilon \varepsilon_0 k_b T / 2 C_0^* z^2 e^2}$ and the thermal potential $\varsigma = k_b T / ze$. Here k_b and T are Boltzmann constant (1.38×10^{-23} J/K) and absolute temperature, respectively.

The resulting non-dimensional equations are listed below.

$$\nabla^2 \psi = -\rho_e, \tag{5a}$$

$$\rho_e = C^+ - C^-, \tag{5b}$$

$$\frac{\partial C^\pm}{\partial t} = \nabla^2 C^\pm \pm \gamma \nabla \cdot \left(C^\pm \nabla \psi\right), \tag{6}$$

$$\nabla \cdot \mathbf{V} = 0, \tag{7}$$

$$\frac{\partial \mathbf{V}}{\partial t} = -\nabla P + Sc \nabla^2 \mathbf{V} - \beta \rho_e \left(\nabla \psi\right). \tag{8}$$

Here, $\gamma = \left(d / \lambda_d\right)^2 / 2$ represents the relative size of the electrode based on λ_d and $Sc = \mu / \rho D$ is the Schmidt number. Further, $\beta = \gamma Sc\left(\psi_{ref} / V_{apo}\right)$ is a dimensionless parameter characterizing the electrical body force. When AC field is applied to the electrodes the time period of AC potential is taken as the reference time, i.e., $t^* = t / f$ and correspondingly the nondimensional quantities are modified.

With the assumption of insulated walls and ideally polarizable electrodes, the suitable boundary conditions for the potential and the concentration in the non-dimensional forms are listed below.

On walls:

$$\frac{\partial \psi}{\partial n} = 0, \tag{9}$$

$$\frac{\partial C^\pm}{\partial n} = 0. \tag{10}$$

On electrodes:

$$\psi = \begin{cases} V_{apo} / \psi_{ref}^* & \text{for DC} \\ \left(V_{apo} / \psi_{ref}^*\right) \sin(2\pi t) & \text{for AC} \end{cases} \tag{11}$$

$$\frac{\partial C^\pm}{\partial n} \pm \gamma \left[C^\pm \frac{\partial \psi}{\partial n}\right] = 0, \tag{12}$$

where n indicates the local coordinate normal to the corresponding surface. No-slip and impermeable boundary conditions for velocity are applied on both walls and electrodes.

3. Numerical schemes

The numerical simulation of ion transport is challenging due to the strong coupling among each of the Poisson-Nernst-Planck (PNP) equations. So the decoupled method for solving these equations requires very small time step to avoid the instability in the numerical process. We have solved the PNP equations in both decoupled and coupled ways. In the decoupled method, the Poisson equation is first solved using the ICCG (incomplete Cholesky conjugate gradient) algorithm. Then the NP equations are solved using finite-volume-based fractional-step method. The diffusion term in the NP equations is treated implicitly, while the nonlinear conduction term is treated explicitly. Enough care is taken to maintain second order accuracy of the discretized equations. The resulting banded matrix of algebraic equations is solved using ICCG iteration technique. The immersed boundary (IB) scheme used

for imposing the no-flux condition of concentration in the decoupled solver is detailed later in this section. We have also developed a coupled methodology to solve the PNP equations in a fully implicit way. The nonlinear conduction term in the NP equations is linearized by the Newton-Raphson method. The multi-diagonal asymmetric banded matrix resulting from the discretization of the coupled PNP equations is then solved using CGSTAB iteration technique. But the coupled solver developed is applicable only to rectangular electrodes, where the electrode boundary coincides with the grid lines. Here the ionic flux crossing the electrode boundary can be set to zero directly in the numerical process as the boundary is coinciding with the finite volume element boundary. Finite-volume-based fractional-step method is used for the solution of Stokes equations. The no-slip, impermeable boundary conditions for the velocity on the immersed electrodes are treated by using discrete forcing IB methodology given in Kim et al. [19].

The Robin type concentration boundary condition on the electrodes is presented by Eq. (12) in the nondimensional form. However, it is not so easy to apply it in the numerical computation, especially for the cylindrical electrodes where the boundary does not coincide with the grid points. We have developed a simple and easy method by extending the basic concept of IB method given in Kim et al. [19]. To satisfy the boundary condition (12) we add a forcing term to the NP equations for the solid grids near the boundary:

$$\frac{\partial C^{\pm}}{\partial t} = \nabla^2 C^{\pm} \pm \gamma \nabla \cdot \left(C^{\pm} \nabla \psi \right) + f_{c\pm} , \tag{13}$$

The concentration forcing term $f_{c\pm}$ is zero everywhere in the domain except near the immersed boundary. Fig. 2 is prepared to explain the procedure of evaluating the concentration forcing. Using Eq. (13), we calculate $f_{c\pm}$ in an explicit way as follows:

$$\begin{aligned} (f_{c\pm})^n = & \frac{(\hat{C}^{\pm})^n - (C^{\pm})^{n-1}}{\Delta t} \\ & - \left[\nabla^2 (C^{\pm})^{n-1} \pm \gamma \nabla \cdot ((C^{\pm})^{n-1} \nabla \cdot \psi^{n-1}) \right], \end{aligned} \tag{14}$$

where $\hat{C}^{\pm}$ is unreal concentration defined at the forcing point (point "S" in Fig. 2). The concentration $\hat{C}^{\pm}$ is determined in such a way that the no-flux boundary condition is satisfied on the electrode surface "B". To do so, we first assume that the transient term of Eq. (10) is negligible in the region adjacent to the electrode and thus Eq. (12) is applicable for this region too. Integration of Eq. (12) gives:

$$(\hat{C}^{\pm})^n = A^{\pm} \exp(\mp \gamma \psi^{n-1}) , \tag{15}$$

where the integration constant, $A^{\pm}$, is supposed to remain invariant in the EDL region along the normal to the electrode surface. This means we can compute $A^{\pm}$, to be used for boundary condition at the wall (point "B" in Fig. 2), by using

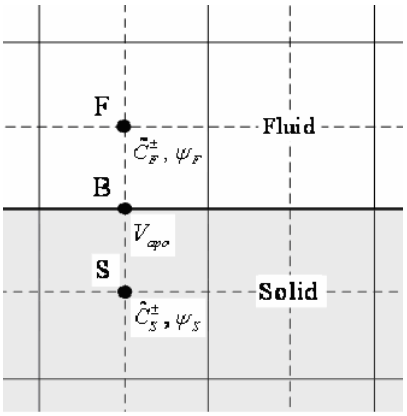

(a)

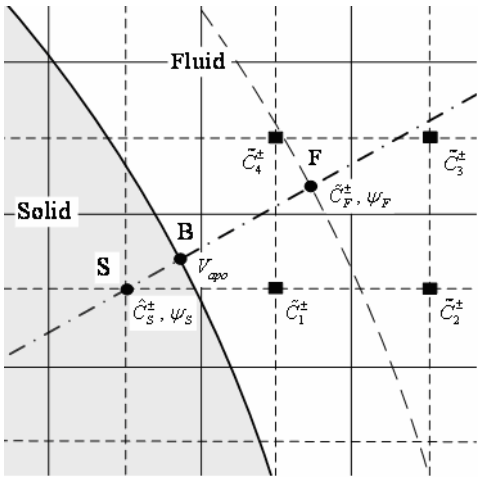

(b)

Fig. 2. Schematic diagram of the interpolation scheme for the concentration forcing for the case of (a) rectangular and (b) circular electrodes.

the variables at the fluid points (point "F" in Fig. 2) with the following equation:

$$A^{\pm} = (\tilde{C}_F^{\pm})^n \exp(\pm \gamma \psi_F^{n-1}) , \tag{16}$$

where the subscript 'F' denotes the interpolation point (see Fig. 2(b)) defined as the intersection of the normal line to the boundary drawn through the forcing point "S" with the offset boundary drawn by a dashed line in the figure. The '~'symbol indicates that the quantity is evaluated explicitly. $(\tilde{C}^{\pm})^n$ is obtained by using the following equation:

$$\frac{(\tilde{C}^{\pm})^n - (C^{\pm})^{n-1}}{\Delta t} = \nabla^2 (C^{\pm})^{n-1} \pm \gamma \nabla \cdot ((C^{\pm})^{n-1} \nabla \cdot \psi^{n-1}) , \tag{17}$$

Fig. 2(a) shows a regular boundary coinciding with the grid line for the case of rectangular electrodes; as a result there is no need for any interpolation for this case. For a curved

boundary (see Fig. 2(b)) we use 2nd order bi-linear interpolation to calculate the concentration $\tilde{C}_F^{\pm}$ and the potential ψ_F at 'F' and linear extrapolation to calculate potential ψ_S at 'S'.

The complete procedure of determining concentration forcing is given below.

(1) Update the concentrations $\tilde{C}_1^{\pm}$, $\tilde{C}_2^{\pm}$, $\tilde{C}_3^{\pm}$ and $\tilde{C}_4^{\pm}$ explicitly using Eq. (17).
(2) Calculate $\tilde{C}_F^{\pm}$ and ψ_F using the bi-linear interpolation scheme.
(3) Determine the constant $A^{\pm}$ using Eq. (16).
(4) Determine ψ_S by the linear extrapolation scheme with the values V_{apo} and ψ_F.
(5) Calculate $\hat{C}_S^{\pm}$ at the forcing point using Eq. (15) with $A^{\pm}$ value determined in item 3 above.
(6) Calculate $f_{c\pm}$ using Eq. (14).

The accuracy the concentration-forcing scheme can be improved by using a second-order polynomial for extrapolation of ψ_S.

4. Results and discussions

The governing equations are solved numerically for the domain shown in Fig. 1(b). The electrolyte used in the present study is dilute potassium chloride (KCl) solution of 1μM concentration. The thickness of the electric double layer at this concentration is of the order of 300 nm, which can be resolved effectively with the suitable number of grids. We set the diffusivity of the ionic species K^+ and Cl^- at 10^{-9} m^2/s. The relative permittivity of the electrolyte is taken as 80. For DC electroosmotic study, the potentials on the anode and cathode are maintained at ±0.025 V. A uniform staggered grid of 200×100 is selected in the analysis after the grid independence of the results is confirmed. Three different grid numbers, 200×100, 300×150 and 400×200, were considered in the grid convergence test and it is found that the improvement in the results is negligible for higher grid-resolution. A nondimensional time step of 10^{-3} is used in the analysis.

4.1 Numerical validation

The correctness of the numerical codes developed in this study is first ensured by comparing the results obtained by the fractional-step based decoupled solver with those obtained from the coupled solver for the rectangular electrodes. Fig. 3(a) shows distribution of the steady-state cation-concentration along horizontal centre line in the domain. The solid line shows the results obtained from fractional-step based decoupled solver and the dashed line those obtained using the coupled solver. The IB methodology described in the section 3 is used to impose the concentration boundary conditions on the electrodes in case of decoupled solver. Fig. 3(b) shows the comparison of steady-state potential distributions along the horizontal centerline. The good agreement between the two results guarantees the validity of the numerical code. During the transients it is found that the center facing-sides of the electrodes get charged faster than the other; this is due to the stronger field present in that region.

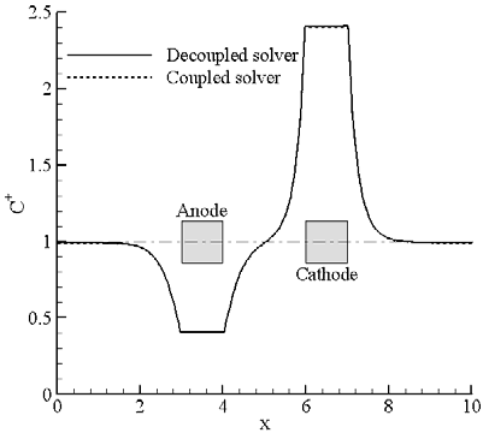

(a)

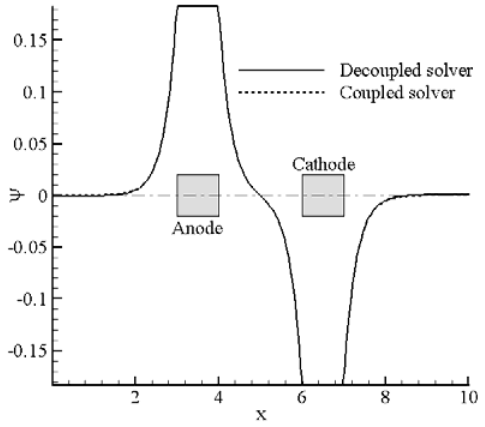

(b)

Fig. 3. Comparison of numerical results of decoupled and coupled solvers; distributions, along the horizontal centerline, of (a) nondimensional cation concentration and (b) nondimensional potential.

Numerical experiments have been performed to verify how exactly the numerical solutions satisfy the governing equations. The various terms (conduction, diffusion and transient) of the governing equations are computed and balanced to calculate the absolute error. The numerical experiments are conducted at arbitrary points close to the electrode and at different time intervals. The absolute error associated with numerical solution is found to be negligible, suggesting the high accuracy of the numerical results.

To further ascertain the accuracy of the new IB method, we also compared the numerical results with those obtained from the Poisson-Boltzmann model. By making quasi-steady assumption in the NP equations (6), the expression for the ionic concentration distribution over a charged surface is obtained as $C^{\pm}=\exp(\mp\gamma\psi)$. The Poisson-Boltzmann equation governing the induced electric potential in the radial direction, around a charged cylinder in an unbounded electrolyte takes the following form:

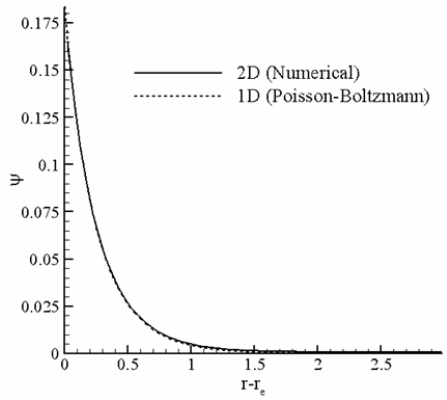

Fig. 4. Comparison of numerical results of decoupled solver with the Poisson-Boltzmann model; variation of induced potential from the surface of the left electrode in the negative x direction at steady state.

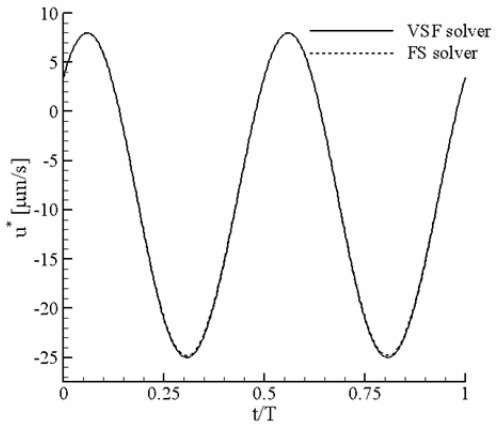

Fig. 5. Comparison of time evolved horizontal velocity at a point (x, y) = (4.0, 3.1) under AC field for the rectangular electrodes, obtained from fractional-step based primitive-variable solver and vorticity-stream-function based solver.

$$\frac{1}{r}\frac{d}{dr}\left(r\frac{d\psi}{dr}\right)=2\sinh(\gamma\psi)\ . \tag{18}$$

The above nonlinear differential equation is linearized using Taylor's series expansion and solved using iterative procedure. Fig. 4 shows the comparison of the results for induced potential distribution from the surface of the electrode in the radial direction. The excellent agreement between the two results confirms the accuracy and validity of our code.

Earlier, a fractional-step (FS) based primitive-variable Navier-Stokes solver was developed to study the flow over a circular cylinder [20]. The angle of separation and the wake length for different Reynolds numbers were compared with the results available in the literature. We found our results are in good agreement with those obtained by Guo et al. [21]. The code was then modified to solve the Stokes equations by dropping the inertia terms for the cases of both the circular and rectangular electrodes. Also a new code was developed to solve Stokes equations using vorticity-stream-function (VSF) method for the case of rectangular electrodes. The numerical

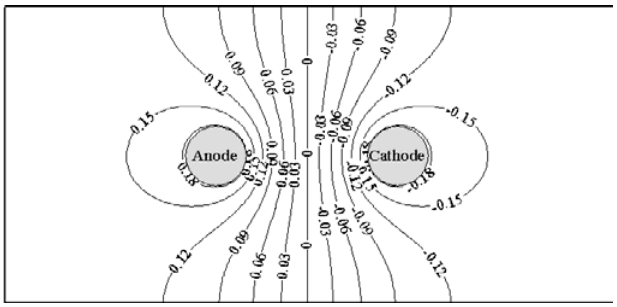

Fig. 6. Initial distribution of the iso-potential (nondimensional) lines around the electrodes under DC field.

results obtained from the FS based solver were compared with those obtained from VSF based solver. Fig. 5 shows the time evolution of horizontal component of the electroosmotic velocity at a point (4.0, 3.1) during a cycle of AC. The point is located in the region right top of the left electrode. Both the solvers predict the same velocities, proving the reliability of the numerical code. Also, we can observe here that the velocity completes two harmonics for one AC period. The reason for this is that during the first quarter of the AC cycle the potential on the anode increases, causing anions to move towards it; while during the next quarter the potential decreases, causing these ions to move away. Similarly, during the second half cycle of AC the anode becomes switched to cathode, attracting cations in the third quarter and repelling them during the fourth quarter.

4.2 DC electroosmosis around circular electrodes

The results of ion transport and electroosmotically induced flow field when the DC field is applied to the circular electrodes are discussed in this section. The distribution of the electrical potential in the domain immediately after the electric field is applied is shown in Fig. 6. The potential distribution shows the existence of a strong field in the region between the two electrodes. As soon as the electric field is applied, the free ions in the electrolyte start migrating towards the electrode of opposite polarity and away from the electrode of same polarity. It is observed during the transient that the sides of the electrodes facing to the center of the domain get charged first and then slowly the other region around the electrode. The conduction force acting on the ions brings them towards the electrode surface from the bulk. Initially, the gradient of concentration is zero, so the effect of diffusion term is negligible. Once the EDL is charged, there will be a net diffusion of ions from the EDL towards the bulk. Finally, the system attains a steady state, where the ionic conduction is balanced by the diffusion in the opposite direction.

The steady state nondimensional counter-ion (cation) concentration distribution and the induced electrical potential distribution around the cathode are shown in Fig. 7. The iso-concentration lines for the cationic species are concentric and their spacing indicates the steepness of the gradients around the electrodes. An identical distribution of counter-ions (ani-

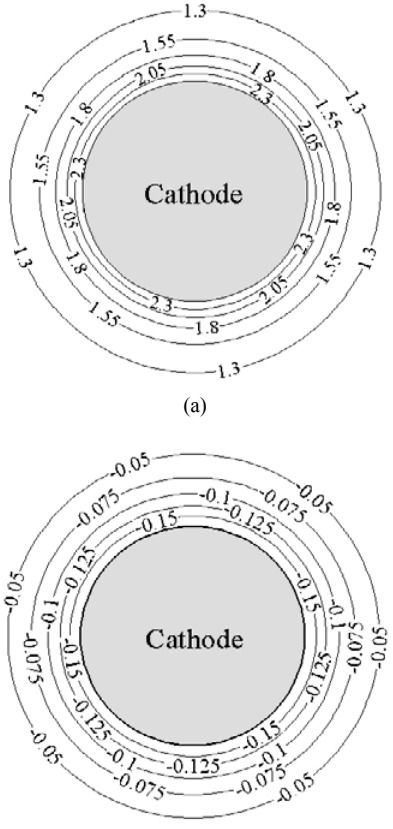

(a)

(b)

Fig. 7. The iso-potential and iso-concentration lines around the circular electrodes depicting EDL around them under DC field; (a) steady state cation concentration distribution and (b) steady state potential distribution around the cathode.

ons) is observed around the anode. The anion concentration distribution in the EDL of an electrode can be related to the cation concentration as follows: $\ln(C^-) = -\ln(C^+)$. In the region beyond the EDL, at steady state the induced electrical potential is zero and concentration of the cationic and the anionic species is equal to 1.

The migration of ions due to conduction force during EDL charging drags the surrounding fluid along, setting an electroosmotic flow. But as soon as the steady state is reached, this induced charge electroosmotic flow disappears, because the electrodes are completely screened by counter-ions and so there are no ionic movements. Fig. 8 shows time evolution of flow velocities and ionic concentrations at a point (4.4, 2.5) located on the right side of the anode. In the figure we can clearly see the disappearance of the flow field as the screening of electrodes completes. Initially, in the absence of net diffusion, the fluid velocity increases sharply due to conduction of ions towards the electrodes. Once the ion diffusion in the opposite direction to the conduction direction starts, the fluid velocity reduces. Finally, the fluid comes to rest in almost the same time the electrodes are screened. Here the velocity diffusion takes place much faster than the ion diffusion as the characteristic time of viscous diffusion is of the order of μs for the

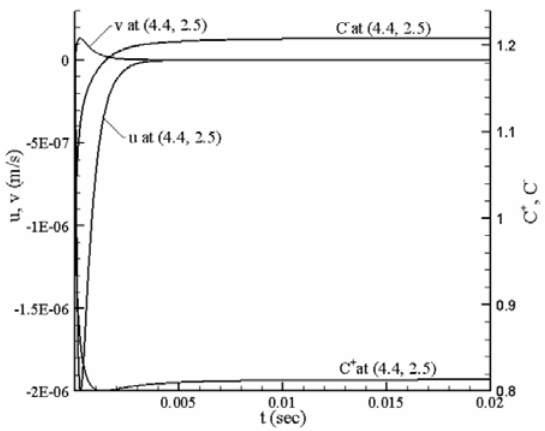

Fig. 8. Time evolution of flow velocities and ion concentrations at a point (x, y) = (4.4, 2.5) for circular electrodes under DC field.

system under study. Thus, to have a continuous fluid flow around the electrodes in the present system, the electric field on the electrodes must be changed periodically by applying AC.

We can see from Fig. 8 that the electroosmotic flow persists approximately for 5 ms. This can be understood through a scale analysis. The process of repulsion of co-ions and accumulation of counter-ions is termed as EDL charging. Generally, the EDL charging time is a function of the electrolyte concentration. The characteristic EDL charging time is given by Debye time $\tau_D = (\lambda_D)^2 / D$. But recently some researchers (e.g. [11]) argued that the characteristic time of EDL charging is a function of both Debye length and the geometric length. They gave the expression for the characteristic time from Laplace transform analysis of transient NP equations as $\tau_c = \lambda_D L / D$, where L is the distance between the parallel plate electrodes [11]. For the cylindrical electrode system shown in the Fig. 1(b), the distance between the points on the electrode surfaces is not constant as in the case of parallel plate electrodes. The nearest points on the electrode are separated by a distance 2μm and the farthest points by 4μm. The rate of EDL charging depends on the position around the electrode, because the strength of the electric field varies with the position on the electrode. The center facing sides gets charged first while the opposite sides last. Thus based on average distance the characteristic time of EDL charging τ_c comes out to be approximately 0.90 ms. Then, this time is of the same order of magnitude as 5.0 ms measured from Fig. 8, implying that τ_c is more appropriate than τ_D (0.094 ms) in predicting the duration of DC electroosmotic flows.

4.3 AC electroosmosis around circular electrodes

AC electroosmosis is quite interesting compared to DC. In this case the potential on the electrodes is changed sinusoidally according to the function: $\psi^* = \pm V_{apo} \sin(\omega t)$, where ω is the angular frequency of the AC. The maximum amplitude of the applied potential is set equal to 0.05 V. The fluid flow

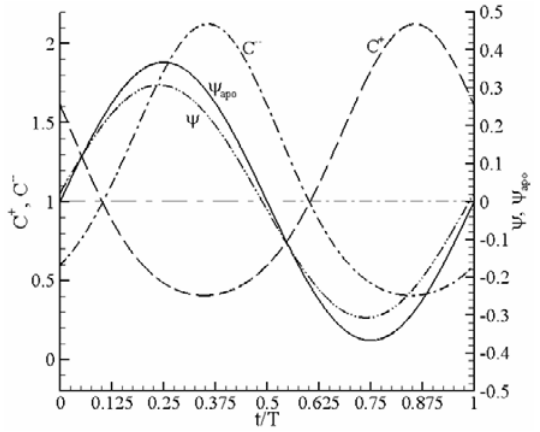

Fig. 9. Variation of potential and concentration at a point (x, y) = (4.1, 2.5) near the left electrode during an AC period for circular electrodes.

under AC strongly depends on the frequency of the applied field. For coplanar electrodes the predominant fluid flow has been observed for the frequencies below the reciprocal of the charge relaxation time [22-24]. For the dilute electrolyte considered in the present study the charge relaxation time $\left(\tau_r = \varepsilon\varepsilon_0/\sigma\right)$ is 9.5×10^{-3} sec, where σ is electrolytic conductivity. So in the present study we have fixed the frequency of the AC potential to 1000 Hz.

The system attains a steady periodic state in approximately 10 periods. The results given in this section are from the tenth period. As in case of DC the free ions in the electrolyte experience a conduction force when the electric field is applied and start migrating towards the electrodes of counter polarity. But with the potential on the electrodes changing periodically, the ions also change their direction of motion periodically with the same frequency of AC potential. Fig. 9 shows the time evolution of the ionic concentration as well as induced electrical potential at a point (4.1, 2.5) located on the right side of the left electrode, during an AC period. The accumulation of counter ions lags the response of the potential on the electrodes by a certain time, which reflects the capacitor nature of EDL. The anion and cation concentration curves are identical with a phase difference of half period between them. The ions far away from the electrodes experience almost no force from the applied electric field, so the ionic concentration near the surrounding walls remains almost invariant.

Fig. 10(a) shows the distribution of the electric potential and Fig. 10(b) the distribution of cationic concentration along the horizontal center line at eight different instances during one AC period. It can be observed that although at the instants T/2 and T the potential on the electrodes is zero, the potential in the domain is not zero. This is again due to the lagging of the charge accumulation on the electrodes due to the capacitor nature of EDL. Differences in concentration gradients in the EDL on the either sides of the electrodes are observed in Fig. 10(b). A larger number of ions accumulate on the center facing-sides of the electrodes due to the stronger field present in that region than the other side. Unlike the ions in the other

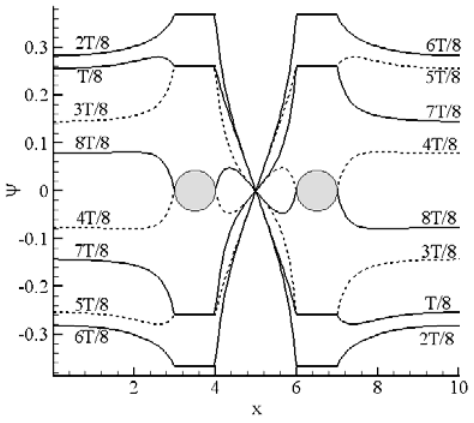

(a)

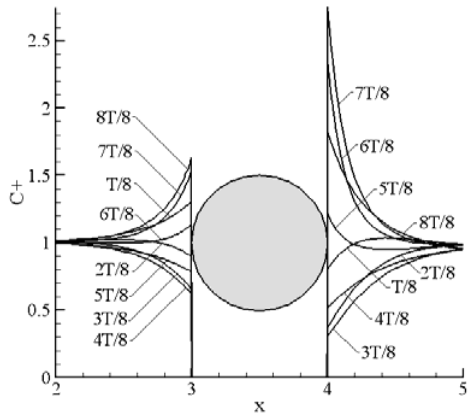

(b)

Fig. 10. The distribution of variables along the horizontal center line during different instances of an AC period; (a) electric potential and (b) cation concentration for the left electrode (distribution is anti-symmetric at the right electrode).

region, the ions in the central region between the electrodes experience two forces. One is the force of attraction towards the electrode of opposite polarity, and the other is the force of repulsion from the electrode of the same polarity.

Unlike the DC case, a continuous non-zero fluid flow persists in the case of AC. The fluid flow is induced due to the Coulomb force acting on the net charge in the EDL. It is observed that the instantaneous flow field completes two harmonics during one AC period. Fig. 11 shows the streamline plots of the flow field during eight different instances of an AC period. The streamlines show that the flow patterns during the second half of the AC period are identical to the ones during the first half period. It can be seen from the instantaneous flow field that the flow from the center of the domain toward the electrodes (Fig. 11(b) and (c)) is stronger than the reverse flow (Fig. 11(a) and (d)). As a result, a net time-averaged continuous flow is sustained in the domain.

Unlike the DC case, a continuous non-zero fluid flow persists in the case of AC. The fluid flow is induced due to the Coulomb force acting on the net charge in the EDL. It is ob-

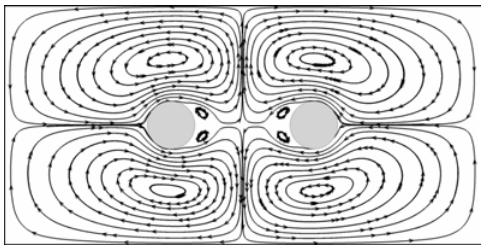

(a) T/8, 5T/8

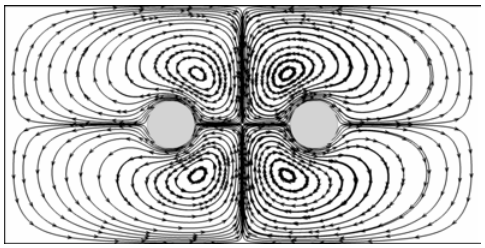

(b) 2T/8, 6T/8

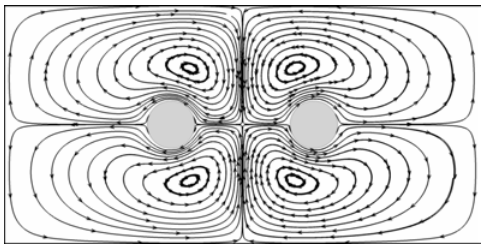

(c) 3T/8, 7T/8

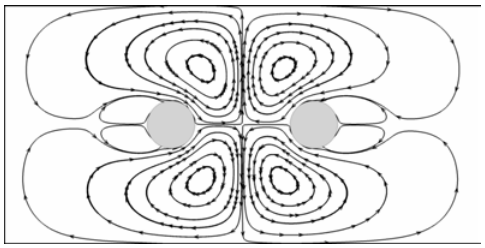

(d) 4T/8, 8T/8

Fig. 11. Streamline plots showing the variation of instantaneous flow field during an AC period. (streamline values are different for each plot).

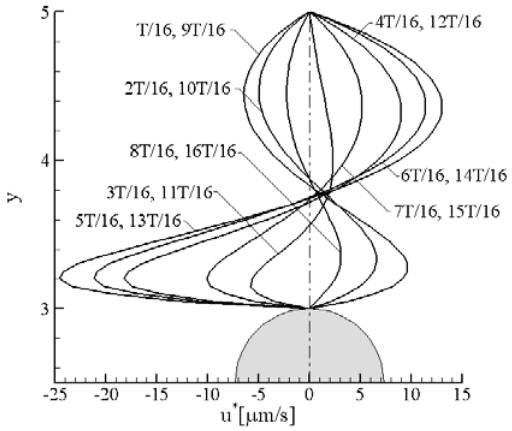

Fig. 12. Time evolution of the horizontal velocity profile along the upper-half vertical centerline of the left electrode; the profile along the lower-half is symmetric with this.

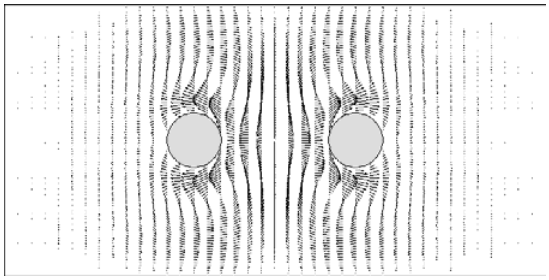

(a)

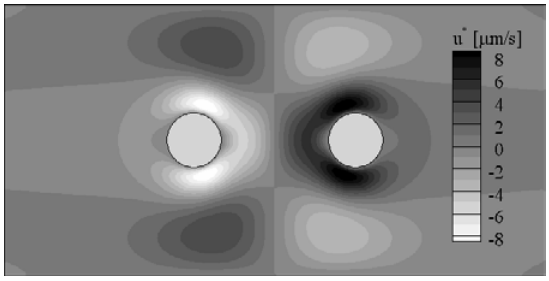

(b)

Fig. 13. Time-averaged flow field; (a) velocity-vector plot and (b) contour of the magnitude of the horizontal velocity.

served that the instantaneous flow field completes two harmonics during one AC period. Fig. 11 shows the streamline plots of the flow field during eight different instances of an AC period. The streamlines show that the flow patterns during the second half of the AC period are identical to those during the first half period. It can be seen from the instantaneous flow field that the flow from the center of the domain toward the electrodes (Fig. 11(b) and (c)) is stronger than the reverse flow (Fig. 11(a) and (d)). As a result, a net time-averaged continuous flow sustains in the domain.

Fig. 12 shows the instantaneous horizontal velocity profiles along the vertical line through the center of the left electrode. Clearly, the flow towards the left is stronger than the one towards the right in the region close to the electrode and vice versa in the region near the top and bottom walls.

The time-averaged flow field is shown in the Fig. 13. Velocities of the order of 10 μm/s are observed. The flow pattern shows four recirculation vortices around the electrodes. This steady flow can effectively enhance the mixing in case of microchannels.

5. Conclusions

The ion transport and electroosmotically induced flow around the cylindrical electrodes are studied by numerical simulation. The PNP equations governing ion transport are

solved using the FS based decoupled solver. The electroosmotically induced flow field is obtained by solving Stokes equations. Using the physics of the problem, a new IB method is developed to impose no flux conditions of concentration on the electrodes. We have also developed a coupled solver for the PNP equations around the rectangular electrodes to ensure the correctness of the decoupled solver with the new IB method for treating the boundary conditions. A comparison of the results has proved that the decoupled solver can predict the ion transport accurately. The only drawback it suffers is the requirement of small time step. The validity of the numerical result is further confirmed by comparing it with the one obtained from the Poisson-Boltzmann model. For the DC case no electroosmotically induced flow field is observed at the steady state. In this case the EDL charging takes less than a millisecond, after which the system remains invariant.

Under AC field the instantaneous flow field oscillates with a frequency double the applied potential. The time average of the flow field over a period AC shows a net flow around the electrodes with four recirculation vortices. This steady lateral flow can be well utilized for enhancing mixing in the case of microchannels.

The effect of frequency on the flow field will be studied in the near future. Also, we want to consider a more practical concentration for the electrolyte in our future study.

Acknowledgment

This work was supported by NRF grant No. 2009-0083510 through Multi-phenomena CFD Engineering Research Center. This work was also supported by a grant No. F0004021-2009-32 from the Information Display R&D Center, one of the Knowledge Economy Frontier R&D Programs funded by the Ministry of Knowledge Economy of Korean Government.

Nomenclature

$C^{\pm}$: Nondimensional concentration
C_0^* : Ionic concentration in the bulk region $\left(\text{no. of ions/m}^3\right)$
D : Diffusion coefficient $\left(\text{m}^2/\text{s}\right)$
d : Electrode size $\left(\text{m}\right)$
e : Electron charge $\left(1.6\times10^{-19}\ \text{C}\right)$
f : AC frequency $\left(\text{Hz}\right)$
F : Faraday constant $\left(96485.3\ \text{C/mol}\right)$
k_b : Boltzmann constant $\left(1.38\times10^{-23}\ \text{J/K}\right)$
P : Nondimensional pressure
R : Universal gas constant $\left(8.314\ \text{J/K mol}\right)$
r : Nondimensional radial distance
r_e : Nondimensional electrode radius
Sc : Schmidt number
T : Temperature $\left(\text{K}\right)$
t : Nondimensional time
U_s : Helmholtz-Smoluchowski velocity $\left(\text{m/s}\right)$
$\mathbf{V}$: Nondimensional velocity vector
$\mathbf{x}$: Nondimensional coordinate vector
z : Valence of ions
ε : Dielectric constant
ε_0 : Permittivity of vacuum $\left(8.85\times10^{-12}\ \text{C}^2/\text{Nm}^2\right)$
ω : Angular frequency of the AC potential $\left(\text{rad/s}\right)$
ς : Thermal potential $\left(\text{Volts}\right)$
ψ : Nondimensional induced electric potential
ρ_e : Nondimensional volumetric electric-charge density
μ : Dynamic viscosity $\left(\text{Ns/m}^2\right)$
λ_d : Debye screening length $\left(\text{m}\right)$
σ : Conductivity of electrolyte $\left(\text{S/m}\right)$

Subscript:

apo : Applied
k : k^{th} ionic species
ref : Reference

Superscript:

$+$: Cation
$-$: Anion
$*$: Quantity in dimensional form

References

[1] R. J. Yang, L. M. Fu and Y. C. Lin, Electroosmotic Flow in Microchannels, *J. Colloid Interface Sci.* 239 (2001) 98-105.
[2] C. Yang, D. Li and J. H. Masliyah, Modeling Forced Liquid Convection in Rectangular Microchannels with Electrokinetic Effects, *Int. J. Heat Mass Transfer*, 41 (1998) 4229-4249.
[3] S. Arulanandam and D. Li, Liquid Transport in Rectangular Microchannels by Electroosmotic Pumping, *Colloids Surf., A,* 161 (2000) 89-102.
[4] J. Alam and J. C. Bowman, Energy Conservation Simulation of Incompressible Electro-Osmotic and Pressure-Driven Flow, *Theor. Comput. Fluid Dyn.* 16 (2002) 133-150.
[5] D. Li, *Electrokinetics in Microfluidics,* Elsevier Academic Press, New York (2004).
[6] R. J. Hunter, *Zeta Poetentials in Colloid Science (Principles and Applications),* Academic Press Inc., London (1981).
[7] L. M. Dumitran, L. Dascalescu, P. V. Notingher and P. Atten, Modeling of Corona Discharge in Cykinder-Wire-Plate Electrode configuration, *J. Electrostat,* 65 (2007) 758-763.
[8] C. T. J. Low, E. P. L. Roberts and F. C. Walsh, Numerical Simulation of the Current, Potential and Concentration distributions along the Cathode of a Rotating Cylinder Hull Cell, *Electrochim, Acta.* 52 (2007) 3831-3840.
[9] Z. Yu and W. Admassu, Modeling of Electrodialysis of Metal Ion Removal from Pulp and Paper Mill Process Stream, *Chem. Eng. Sci.* 55 (2000) 4629-4641.
[10] V. M. Volgin and A. D. Davydov, Numerical Modeling of Non-Steady-state Ion Transfer in Electrochemical Systems with Allowance for Migration, *Russ. J. Electrochem,* 37 (2001) 1197-1205.

[11] M. Z. Bazant, K. Thornton and A. Ajdari, Diffuse-Charge Dynamics in Electrochemical Systems, *Phys. Rev. E.* 70 (2004) 021506.
[12] S. Kang and Y. K. Suh, Numerical Analysis on Electroosmotic Flows in a Microchannel with Rectangle-Waved Surface Roughness using the Poisson–Nernst–Planck Model, *Microfluid, Nanofluid,* 6 (2008) 461-477.
[13] Y. K. Suh and S. Kang, Asymptotic Analysis of Ion Transport in a Nonlinear Regime around Polarized Electrodes under AC, *Phys. Rev. E.* 77 (2008) 031504.
[14] J. Mohd-Yusof, Combined Immersed-Boundary/B-Spline Methods for Simulation of Flow in Complex Geometries. *Annu. Res. Briefs, Center for Turb. Res.,* NASA Ames and Stanford University (1997) 317-327.
[15] E. A. Fadlun, R. Verzicco, P. Orlandi and J. Mohd- Yusof, Combined Immersed Boundary Finite Difference Methods for Three Dimensional Complex Flow Simulations, *J. Comput. Phys.* 161 (2000) 35-60.
[16] W. X. Huang and H. J. Sung, Improvement of Mass Source/Sink for an Immersed Boundary Method, *Int. J. Numer. Methods Fluids,* 53 (2007) 1659-1671.
[17] J. Kim and P. Moin, Application of a Fractional-Step Method to Incompressible Navier-Stokes Equations, *J. Comput. Phys.* 59 (1985) 308-323.
[18] R. Mittal and G. Iaccarino, Immersed Boundary Method, *Annu. Rev. Fluid Mech.* 37 (2005) 239-261.
[19] J. Kim, D. Kim and H. Choi, An Immersed-Boundary Finite-Volume Method for Simulations of Flow in Complex Geometries, *J. Comput. Phys.* 171 (2001) 132-150.
[20] D. V. Fernandes, Y. K. Suh and S. Kang, Immersed Boundary Method for the Analysis of 2D Flow over a Cylinder and 3D Flow over a Sphere, *Proc. KSCFE Autumn Conference*, Daegu, South Korea (2007) 194-199.
[21] Z. Guo, B. Shi and N. Wang, Lattice BGK Model for Incompressible Navier-Stokes Equation, *J. Comput. Phys.* 165 (2000) 288-306.
[22] N. G. Green, A. Ramos, A. Gonzalez, H. Morgan and A. Castellanos, Fluid Flow Induced by Nonuniform AC Electric Fields in Electrolytes on Microelectrodes. I. Experimental Measurements, *Phys. Rev. E.* 61 (2000) 4011-4018.
[23] A. Gonzalez, A. Ramos, N. G. Green, A. Castellanos and H. Morgan, Fluid Flow Induced by Nonuniform AC Electric Fields in Electrolytes on Microelectrodes II, A Linear Double-Layer Analysis, *Phys. Rev. E.* 61 (2000) 4019-4028.
[24] A. Ramos, H. Morgan, N. G. Green and A. Castellanos, AC Electric-Field-Induced Flow in Microelectrodes, *J. Colloid Interface Sci.* 217 (1999) 420-422.

Dolfred Vijay Fernandes received his Bachelor of Engineering (B.E.) in Mechanical Engineering from MAHE University, Manipal, India in 2003. He then completed his Master's degree in thermal sciences specialization from National Institute of Technology, Calicut, India in 2006. Presently he is doing his doctoral studies at Dong-A University, Busan, Korea under the guidance of Prof. Y. K. Suh. His research interests are in the field of computational fluid dynamics, microfluidics and electrokinetics.

Sangmo Kang received his B.S. and M.S. degrees from Seoul National University in 1981 and 1987, respectively, and then worked for five years at Daewoo Heavy Industries as a field engineer. His Ph.D. in Mechanical Engineering is from the University of Michigan in 1996. Dr. Kang is currently a Professor at the Department of Mechanical Engineering at Dong-A University in Busan, Korea. Dr. Kang's research interests are in the area of micro and nanofluidics and turbulent flow combined with the computational fluid dynamics.

Yong Kweon Suh received his B.S. in Mechanical Engineering from Seoul National University, Korea in 1974. He received his Ph.D. degree from SUNY Buffalo in 1986. Dr. Suh is currently a Professor at the Department of Mechanical Engineering at Dong-A university in Busan, Korea. His research interests include electrokinetic phenomena such as electro-osmosis, electrophoresis, motion of magnetic particles, and mixing in micro/nano scales.